Electronic Supplementary Material (ESI) for Nanoscale.

Electronic Supplementary Information (ESI) for:

Detecting the Shape of Anisotropic Gold Nanoparticles in Dispersion With Single Particle Extinction and Scattering

M. A. C. Potenza,[a, ‡] Ž. Krpetić,[b, c ‡] T. Sanvito,[d, ‡] Q. Cai,[b] M. Monopoli,[b] J. M. de Araújo,[b, e] C. Cella,[d] L. Boselli,[b] V. Castagnola,[b] P. Milani*[,a] and K. A. Dawson *[,b]

[a.] CIMAINA and Dipartimento di Fisica, Università degli Studi di Milano, Via Celoria, 16, 20133 Milano, Italy.
[b.] Centre for BioNano Interactions, School of Chemistry and Chemical Biology, University College Dublin, Belfield, Dublin 4, Dublin, Ireland.
[c.] School of Environment and Life Sciences, University of Salford, M5 4WT Salford, United Kingdom
[d.] EOS srl, Viale Ortles 22/4, 20139 Milano, Italy.
[e.] Departamento de Física Teórica e Experimental, Universidade Federal do Rio Grande do Norte, 59078-970, Natal, RN, Brazil

---

‡ These authors have contributed equally: M. A. C. P., Ž. K., T. S.
Present Address: Marco Monopoli, Royal College of Surgeons in Ireland. 121/122 St. Stephen's Green, Dublin 2, Dublin, Ireland. Željka Krpetić, School of Environment and Life Sciences, University of Salford, M5 4WT, Salford, United Kingdom.

* *E.mail: Paolo.Milani@mi.infn.it; Kenneth.A.Dawson@cbni.ucd.ie*

Table of Contents

S1. Anisotropic Gold Nanoparticles – Gold Nanoparticle Shape Library

Table S1. Summary of gold nanoparticles from the nanoparticle shape library used in this work, including details of particle's nominal core diameter based on TEM measurements, shape, and surface functionality.

Sample label	d_{TEM} (nm)	NP Shape	Surface Functionalisation
GNP1	60	Spherical	$HS-(CH_2)_{11}-EG_6-OCH_2-COOH$
GNP2	80	Spherical	$HS-(CH_2)_{11}-EG_6-OCH_2-COOH$
GNS3	60	Branched	$HS-(CH_2)_{11}-EG_6-OCH_2-COOH$
GNP4	124	Branched	$HS-(CH_2)_{11}-EG_6-OCH_2-COOH$
GNP5	92.7 x 39.4	Rod	CTAB/NaOL
GNP6	67.5 x 13	Rod	CTAB/NaOL

Table S2. Growth conditions of gold nanorods: reagent quantities used in the two-step seeded growth reactions.

Sample label	m [CTAC] (g)	m [CTAB] (g)	m [NaOL] (g)	V [$AgNO_3$] (mL) c=4 mM	V [HCl]cc (mL)	Au seeds (mL)
GNP5	N/A	7	1.234	18	1.5	0.4
GNP6	N/A	7	1.234	24	2.1	0.8

Table S3. Growth conditions of branched gold nanoparticles: volumes of reagents utilised in preparations in order to tune the overall diameter of branched gold nanoparticles.

Sample label	V [$HAuCl_4$] (µL)	V [seeds] (µL)	V [Na-citrate] (µL)	V [Hydroquinone] (µL)
GNP3	100	500	250	250
GNP4	100	75	250	250

S2. Modelling the Polarizability of Gold Nanoparticles

Here we present a detailed description of the model that we use to study the role of plasmon resonances in affecting the nanoparticles polarizability and hence the behavior of the SPES results. [1]

Dielectric function and polarizability for gold spheres and ellipsoids

The resonance in the optical cross sections is shifted at the so-called Frölich frequency, [2] which include the effects of both the surface and surrounding medium. Firstly, we notice that for gold the free electron approximation can be assumed to hold for photon energies smaller than 2.2 eV, or a wavelength λ_{min}=560 nm approximately. We used a solid state laser with λ=635 nm, which allows us to neglect bound electrons.[2] We introduce the plasma frequency for bulk (ω_P) and the damping constant (γ). The Frölich frequency in the surrounding medium (ω_F) is affected by the presence of the small layer for stabilisation. This approximation allows us to evaluate the dielectric function $\epsilon = \varepsilon/\varepsilon_0$, where ε_0 is the vacuum dielectric constant. Since $\gamma << \omega_F$ the dielectric function can be approximated by the Drude model (Equation 1) ($i = \sqrt{-1}$ is the complex unit):

$$\epsilon = 1 - \frac{\omega_F}{\omega^2 + i\gamma\omega} \qquad \text{Equation 1}$$

Thanks to the Rayleigh approximation, the polarization of the particle can be obtained on the basis of the electrostatic approximation.

For ellipsoids the polarizability of the particle is then given by Equation 2:

$$\alpha = V\frac{\epsilon - \epsilon_m}{\epsilon_m + L(\epsilon - \epsilon_m)} \qquad \text{Equation 2}$$

where ϵ_m is the dielectric function of the surrounding medium, V the particle volume and L is the geometrical factor corresponding to the orientation considered to evaluate α. This expression reduces to that of a sphere for L=1/3.

In order to interpret the SPES data, we get the scattering amplitude (Equation 3) by following the approach given in literature: [2, 3]

$$S(0) = -ik^3\alpha/4\pi \qquad \text{Equation 3}$$

Here $k = 2\pi/\lambda$.

Under this approximation, the measure of complex amplitude $S(0)$ is directly providing the complex polarizability α we are interested in. More precisely, to interpret our data we refer to a better approximation obtained by expanding the amplitude *S(0)* at the second order by following the approach adopted by van de Hulst.[3] This allows a better description of the real part of the *S(0)*.

Spheres

By using the values $\omega_P = 1.36 \cdot 10^{16}$ Hz and $\gamma = 1.07 \cdot 10^{14}$, [2, 4] we fit the only free parameter, that is the effective refractive index of the functionalisation layer, to the SPES raw data obtained for spheres. The resulting value is n = 1.395 which is reasonable for the material. We, therefore obtain the Frölich frequency of ca. $\omega_F = 6.17 \cdot 10^{15}$ Hz. In Figure S1 we illustrate the scattered fields for spherical nanoparticles with radii between 19 and 41 nm (solid line), compared to the centroids of the experimental results (circles).

Ellipsoids

We inserted the parameters obtained above into the expression for the polarizability of ellipsoids and obtained the scattered field amplitudes $S(0)$.

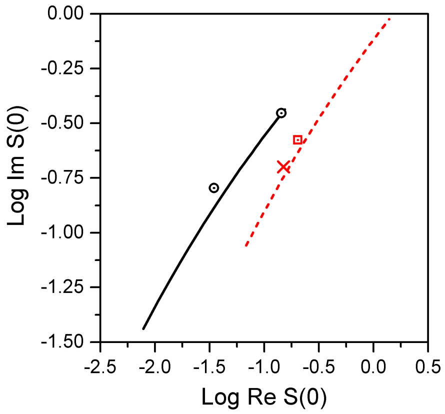

Figure S1: Experimental results for spheres (circles) and rods (square) and the expected behaviour of the field amplitudes for spheres (black solid line) and ellipsoids (red dashed line) with an aspect ratio as in the sample GNP5. With a cross is indicated the expected value for the sample GNP5.

In Figure S1 dashed line outlines the results of our model for ellipsoids with the aspect ratio of 39/93, as in the case of GNP5 (see Table S1), within the range 14×33 – 31×74. The red square represents the centroid of the SPES measurements obtained with the rod sample GNP5, red cross the value obtained from our model for an ellipsoid with semi axes given by the GNP5 size (see below). The experimental shift of the complex field amplitudes is obtained in accordance with the experimental results for rods. Note that our model slightly underestimates the volume, by 15%. This is related to the ellipsoid approximation used, which underestimates the particle volume compared to the actual rod-like shape, having a larger volume for a fixed aspect ratio.

Note that we do not compare the results of our model to the second sample GNP6 because the raw data appreciably extend out of the accessible range of our SPES apparatus. As a consequence, the centroid of the distribution cannot be evaluated properly, and no strong assessment can be done here.

Brownian rotations

We have considered the polarizability of rods, as described by ellipsoids oriented perpendicularly to the direction of the laser beam. However, the particles are oriented randomly, therefore this can appear as an incorrect assumption. By contrast one has to take into account the rotational Brownian motions, having the characteristic times are much smaller than the transit time through the beam (30 μs). The particle is illuminated in many different positions, with the highest probability of being oriented perpendicularly (or almost perpendicularly) to the incoming beam. As a result, the time evolution of the measured intensity values will fluctuate accordingly, and the specific data analysis performed during the generation of the SPES data will favour the measurement with higher values. We can rigorously prove this argument by evaluating the complex field amplitudes expected for particles with an orientation parallel to the beam direction: the expected values are approximately one decade smaller than the others for both the real and imaginary parts. This should spread the SPES raw data by this amount in the plane, which was not observed experimentally (see Figure 3 in the main text). We compare the experimental results to the amplitudes obtained for orientations perpendicular to the direction of the beam.

Branched (Star-shaped) particles

Using again the parameters obtained for spheres, we can interpret the data obtained for star shaped particles. As it has been evidenced, data are appreciably shifted towards larger real parts with respect to spheres and rods. To interpret this shift we note that star particles are characterised by very small structures compared to the size and therefore the surface modes will be strongly changed with respect to spheres. A quantitative simple description is no more possible here, nevertheless limiting the mean free path will increase the damping constant γ. [2] This can be introduced into our model just by limiting the mean free path to dimensions similar to the thin structures of the particles. The imaginary part of the dielectric constant, ϵ'', is increased because of the increase of the damping constant γ. This can be described by adding to the damping constant of the bulk metal the ratio between the electron velocity at the Fermi surface, v_F, divided by the length scale that limits the mean free path, t, [2] For gold v_F= 1.4 10^6 m/s so that it is straightforward to obtain ϵ''. By inserting the complex dielectric constant into the forward scattered amplitude $S(0)$, the ratio R of the real and complex parts of it can be easily written as a function of the length scale t. Limiting again to the first order expansion (the second order term will just increase the real part), the ratio R turns out to have the following dependence on t:

$$R = -3\epsilon_m \frac{\epsilon''}{A+\epsilon''^2} \qquad \text{Equation 4}$$

This expression can be simplified by noting that for gold, $A \gg \epsilon''$. Therefore, the result of limiting the mean free path of electrons in the particle is just to increase the real part of $S(0)$ with respect to the imaginary one, as observed experimentally in our SPES data.

For comparison we report in Table S4 experimental results and the corresponding values expected on the basis of our modelling. Each number is the weighted average of the experimental results shown in the main. Logarithms are reported for a better link to Figure 3.

Table S4. Experimental results *vs* theoretical modelling.

Sample, figure	Log Re S(0) (exp)	Log Im S(0) (exp)	Log Re S(0) (model)	Log Im S(0) (model)
GNP1 (Figure 3.a)	-1.460	-0.796	-1.37	-0.82
GNP2 (Figure 3.b)	-0.844	-0.454	-0.89	0.48
GNP5 (Figure 3.d)	-0.693	-0.576	-0.81	-0.71

S3. Physico-Chemical Characterisation of Anisotropic Gold Nanoparticles

S4.1. Characterisation of Spherical Gold nanoparticles (GNP1)

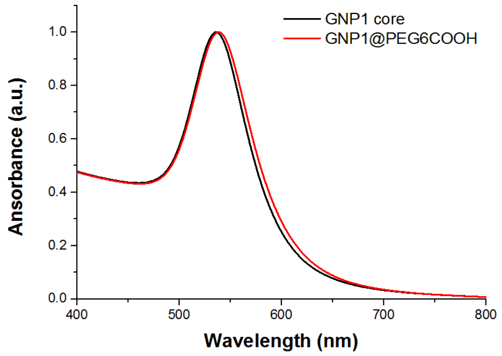

Figure S2. UV-Vis spectra of GNP1 before and after functionalisation with PEG6COOH thiol ligand. Surface Plasmon resonance (SPR) values were 536 nm and 539 nm respectively.

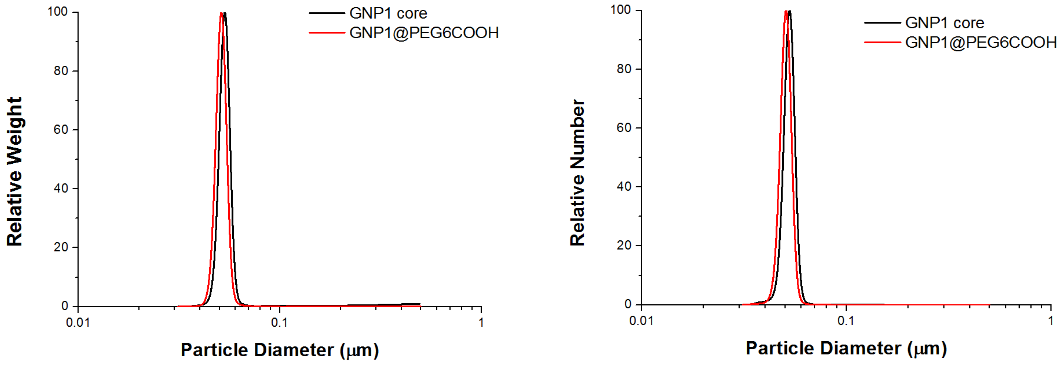

Figure S3. Differential Centrifugal Sedimentation (DCS) measurements of GNP1 before and after functionalisation with PEG6COOH thiol ligand.

Table S5. DCS measurements of particle size distributions reported by weight and number.

	d_{WD} (nm)	Half Width (nm)	d_{ND} (nm)	Half Width (nm)
GNP1 core	53.2	7.6	52.5	7.5
GNP1@PEG6COOH	51.2	7.3	50.6	7.3

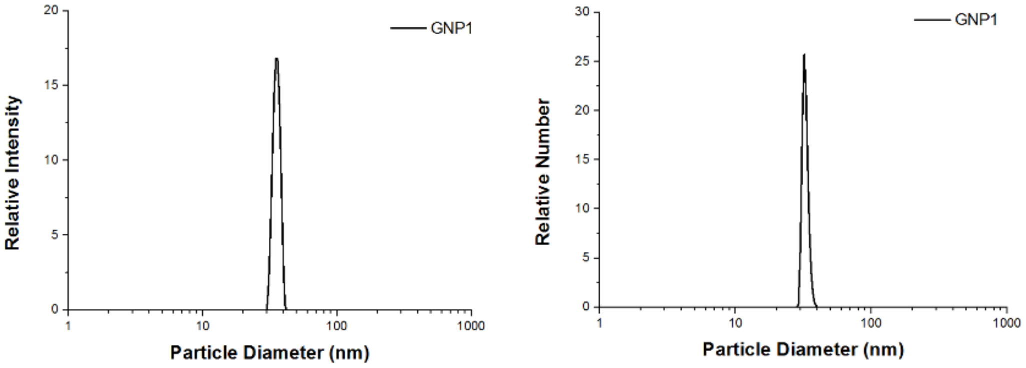

Figure S4. Dynamic Light Scattering (DLS) measurements of GNP1 after functionalisation with PEG6COOH thiol ligand.

Table S6. Particle diameter PDI of GNP1 by DLS.

	Z-Average (nm)	**Particle Diameter by Intensity (nm)**	**Particle Diameter by number (nm)**	**PDI**
GNP1	65.94	74.75	48.84	0.114

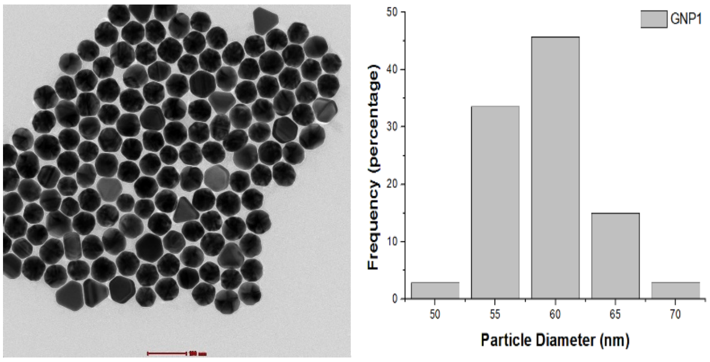

Figure S5. TEM micrographs and particle size distribution chart of GNP1. 140 particles were counted automatically by Image-J. <d>=59 nm. Scale bar is 100 nm.

S4.2. Characterisation of Spherical Gold nanoparticles (GNP2)

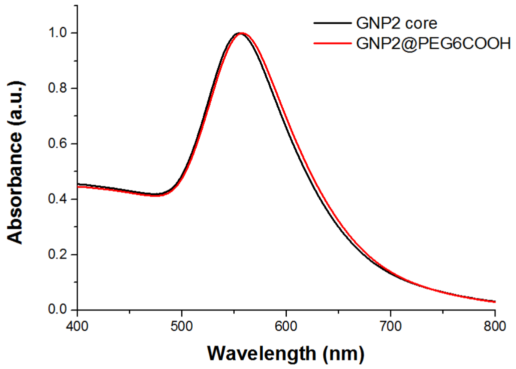

Figure S6. UV-Vis spectra of GNP2 before and after functionalisation with PEG6COOH thiol ligand. SPR values were 555 nm and 558 nm respectively.

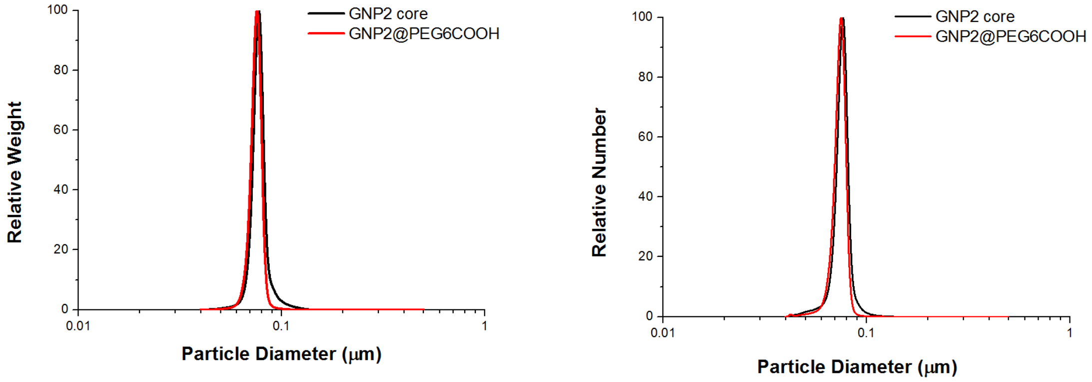

Figure S7. DCS measurements of GNP2 before and after functionalisation with PEG6COOH thiol ligand.

Table S7. DCS measurements of particle size distributions reported by weight and number.

	d_{WD} (nm)	**Half Width (nm)**	**d_{ND} (nm)**	**Half Width (nm)**
GNP2 core	77.1	9.9	76.3	10.2
GNP2@PEG6COOH	75.5	9.7	74.8	10.2

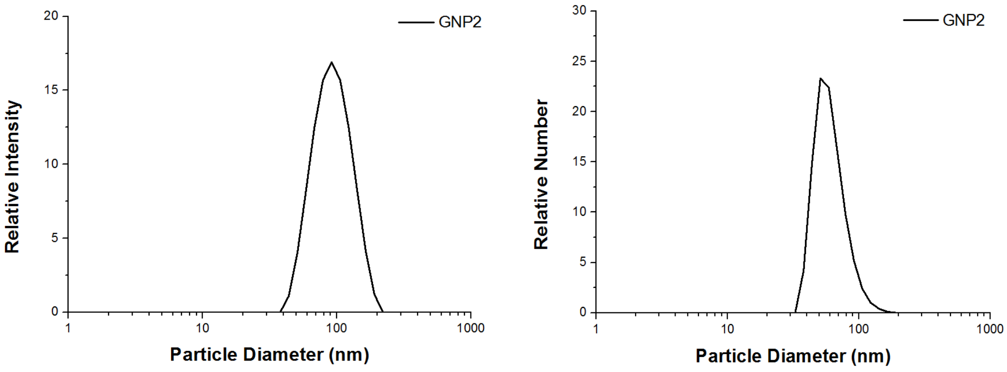

Figure S8. DLS measurements of GNP2 after functionalisation with PEG6COOH thiol ligand.

Table S8. Particle diameter PDI of GNP2 by DLS.

	Z-Average (nm)	**Particle Diametere by Intensity (nm)**	**Particle Diametere by number (nm)**	**PDI**
GNP2	93.05	105.6	67.56	0.112

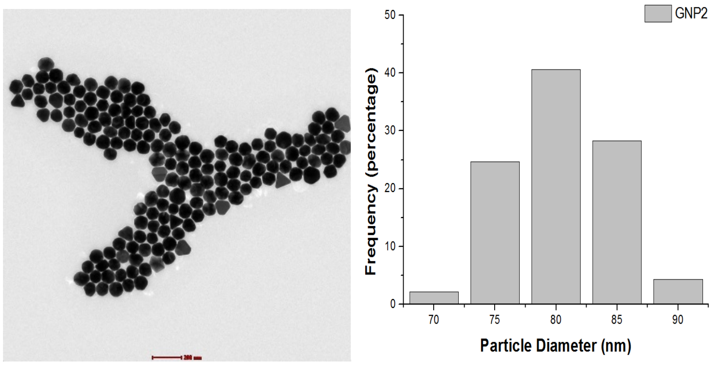

Figure S9. TEM micrographs and particle size distribution chart of GNP2. 138 particles were counted automatically by Image-J. <d>=84 nm. Scale bar is 200 nm.

S4.3. Characterisation of Branched Gold Nanoparticles (GNP3)

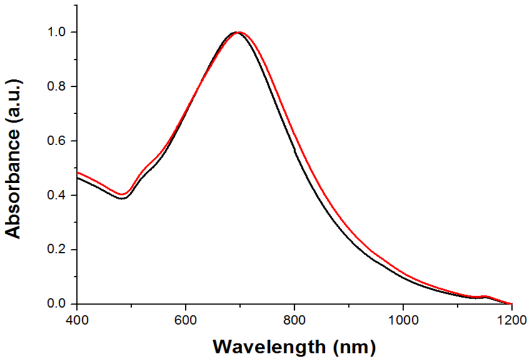

Figure S10. UV-Vis spectra of GNP3 before and after functionalisation with PEG6COOH thiol ligand. SPR values were 692 nm and 700 nm respectively.

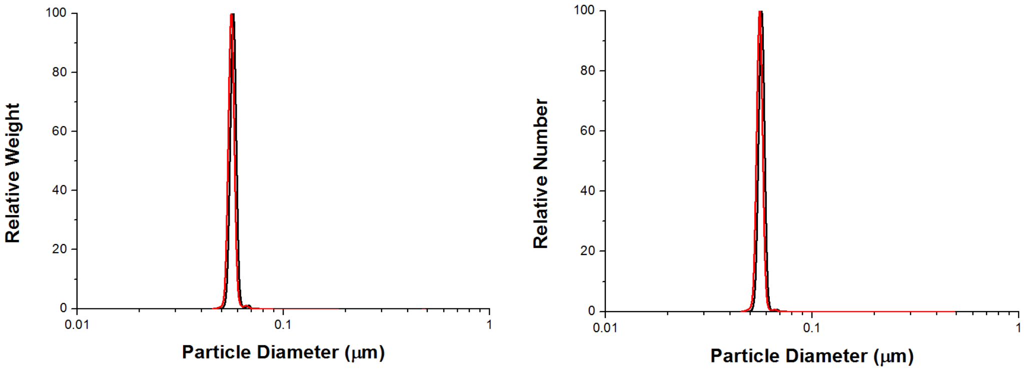

Figure S11. DCS measurements of GNP3 before and after functionalisation with PEG6COOH thiol ligand.

Table S9. DCS measurements of particle size distributions reported by weight and number.

	d_{WD} (nm)	**Half Width (nm)**	**d_{ND} (nm)**	**Half Width (nm)**
GNP3 core	57	4.4	56.9	4.5
GNP3@PEG6COOH	55.8	4.3	55.6	4.3

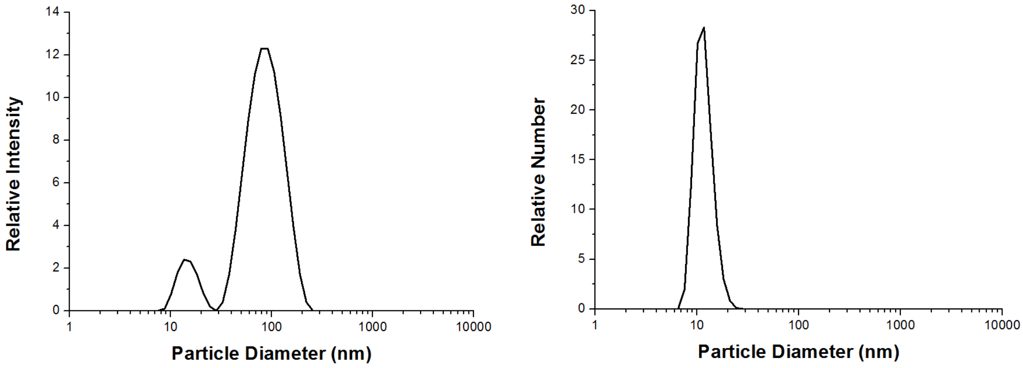

Figure S12. DLS measurements of GNP3 after functionalisation with PEG6COOH thiol ligand.

Table S10. Particle diameter PDI of GNP3 by DLS.

	Z-Average (nm)	**Particle Diameter by Intensity (nm)**	**Particle Diameter by number (nm)**	**PDI**
GNP3	60.8	82.11	11.47	0.283

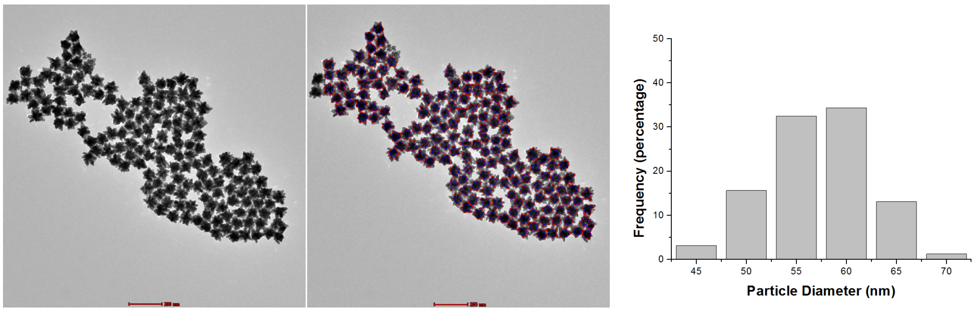

Figure S13. TEM micrographs and particle size distribution chart of GNP3. 160 particles were counted. <d>=57 nm. Scale bar is 200 nm. Particle outlines for counting of branched gold particles obtained by in-house developed method (see Section S5 for further details).

S4.4. Characterisation of Branched Gold Nanoparticles (GNP4)

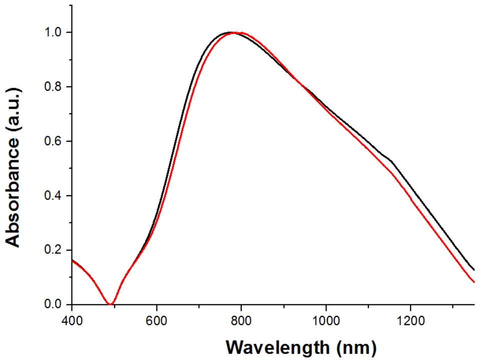

Figure S14. UV-Vis spectra of GNP4 before and after functionalisation with PEG6COOH thiol ligand. SPR values were 771 nm and 801 nm respectively.

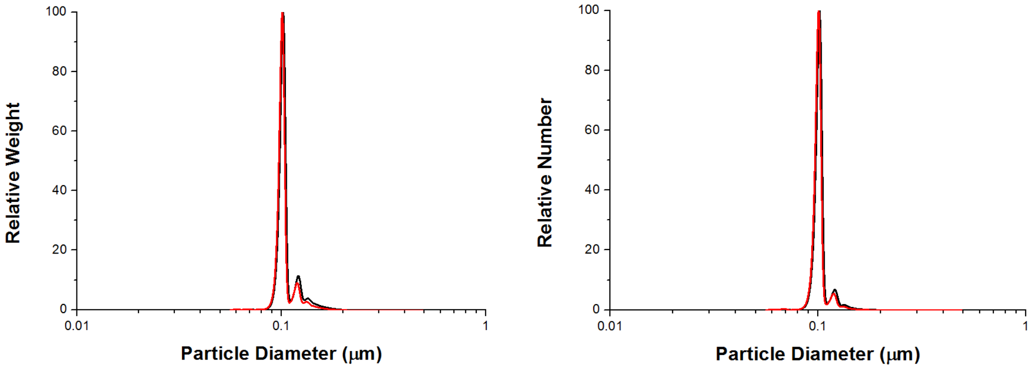

Figure S15. DCS measurements of GNP4 before and after functionalisation with PEG6COOH thiol ligand.

Table S11. DCS measurements of particle size distributions reported by weight and number.

	d_{WD} (nm)	Half Width (nm)	d_{ND} (nm)	Half Width (nm)
GNP4 core	102	7.3	101.5	7.7
GNP4@PEG6COOH	100.7	7	100.7	7.4

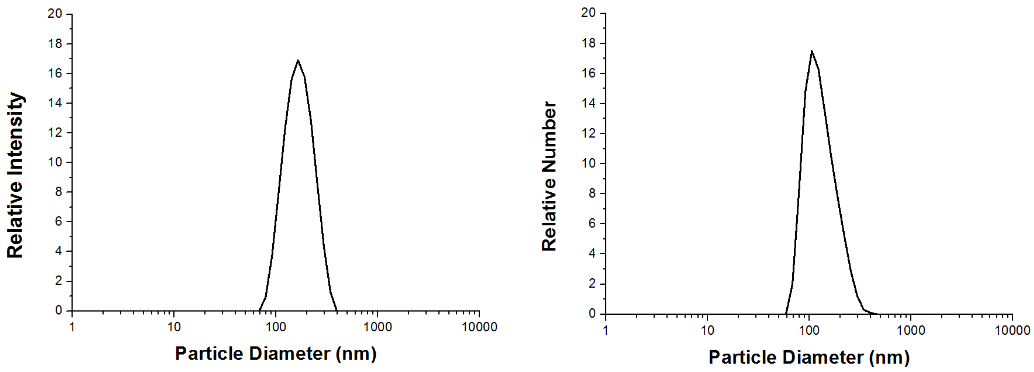

Figure S16. DLS measurements of GNP4 after functionalisation with PEG6COOH thiol ligand.

Table S12. Particle diameter PDI of GNP4 by DLS.

	Z-Average (nm)	**Particle Diameter by Intensity (nm)**	**Particle Diameter by number (nm)**	**PDI**
GNP4	154.1	170.1	133.4	0.085

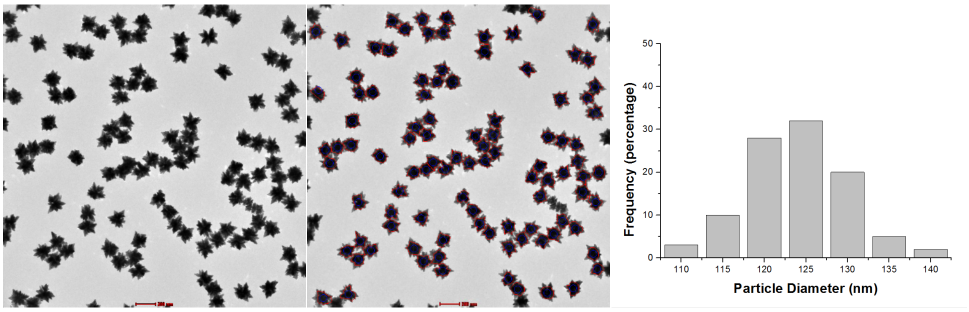

Figure S17. TEM micrographs and particle size distribution chart of GNP4. 100 particles were counted. <d>=124 nm. Scale bar is 200 nm. Particle outlines for counting of branched gold nanoparticles obtained by in-house developed custom method (see Section S5 for details).

S4.5. Characterisation of Rod Shaped Gold Particles (GNP5)

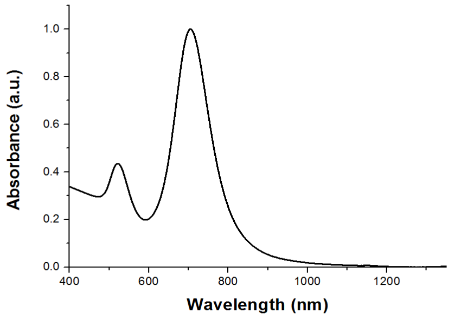

Figure S18. UV-Vis spectra of GNP5. LSPR value was 705 nm.

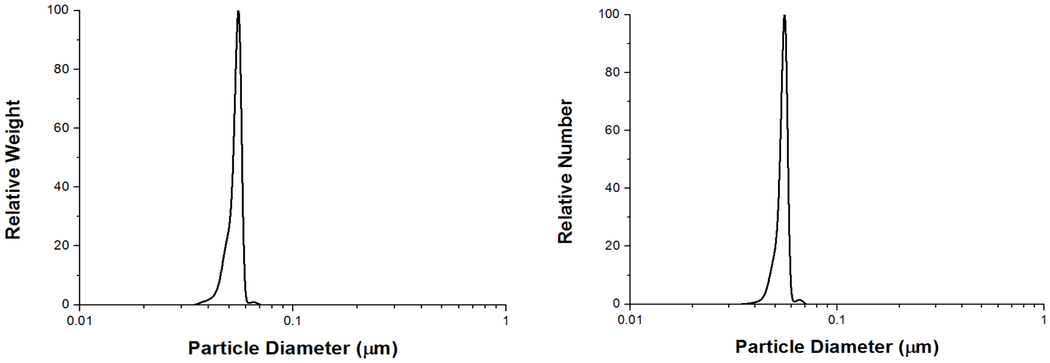

Figure S19. DCS measurement of GNP5.

Table S13. DCS measurements of particle size distributions reported by weight and number.

	d_{WD} (nm)	Half Width (nm)	d_{ND} (nm)	Half Width (nm)
GNP5	55.5	5.1	55.4	5.3

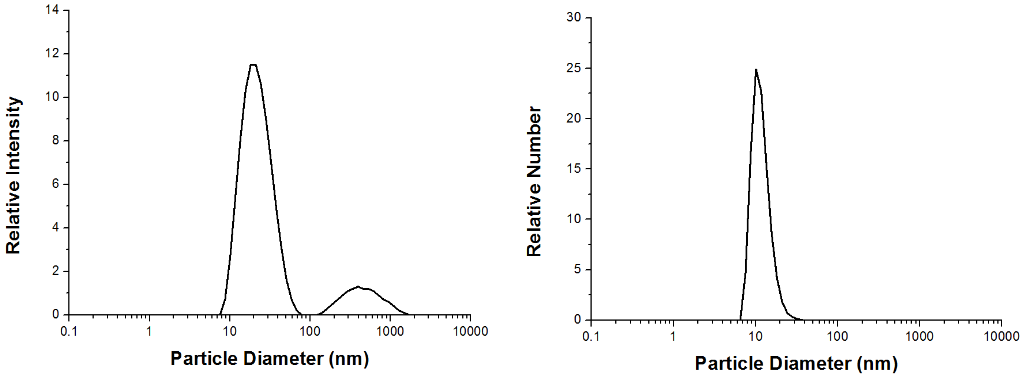

Figure S20. DLS measurements of GNP5.

Table S14. Particle diameter PDI of GNP5 by DLS.

	Z-Average (nm)	Particle Diameter by Intensity (nm)	Particle Diameter by number (nm)	PDI
GNP5	22.15	76.87	11.39	0.31

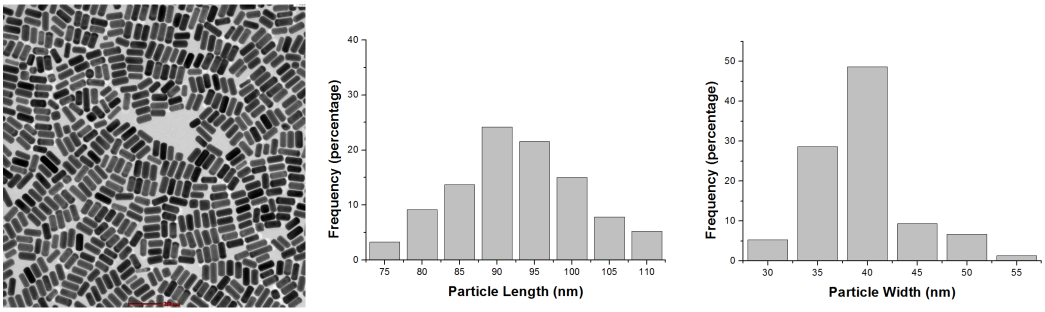

Figure S21. TEM micrographs and particle size distribution chart of GNP5. 153 particles were counted. $<d_{length}>$=92.7 nm, $<d_{width}>$=39.4 nm. Scale bar is 200 nm.

S4.6. Characterisation of Rod Shaped Gold Particles (GNP6)

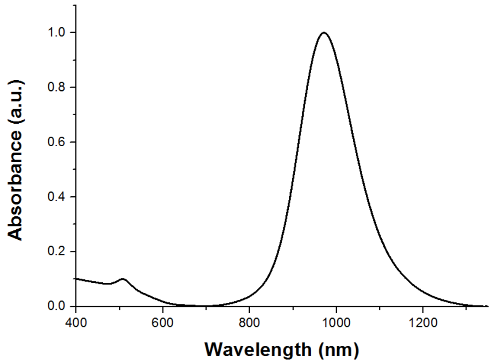

Figure S22. UV-Vis spectra of GNP6. SPR value was 971 nm.

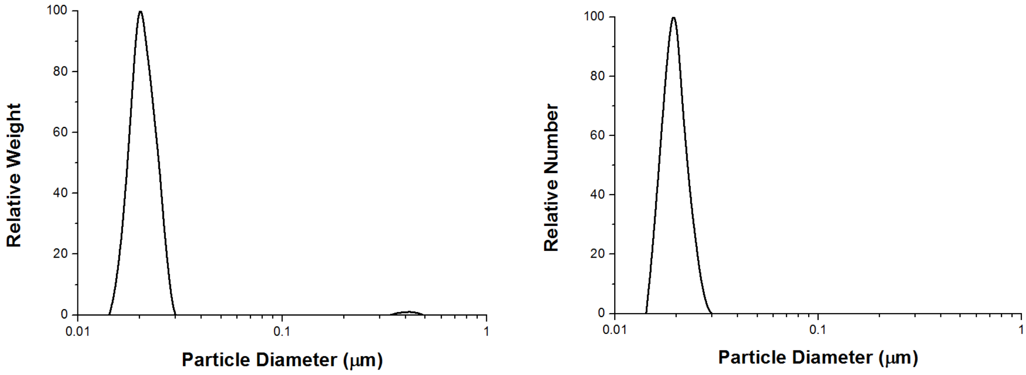

Figure S23. DCS measurement of GNP6.

Table S15. DCS measurements of particle size distributions reported by weight and number.

	d_{WD} (nm)	**Half Width (nm)**	**d_{ND} (nm)**	**Half Width (nm)**
GNP6	20.2	7.5	19.3	6.3

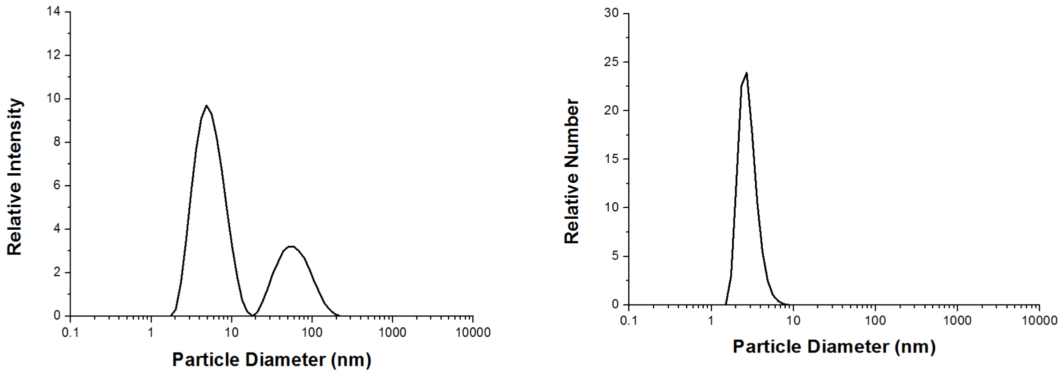

Figure S24. DLS measurements of GNP6.

Table S16. Particle diameter PDI of GNP6 by DLS.

	Z-Average (nm)	**Particle Diameter by Intensity (nm)**	**Particle Diameter by number (nm)**	**PDI**
GNP6	5.476	50.35	2.736	0.244

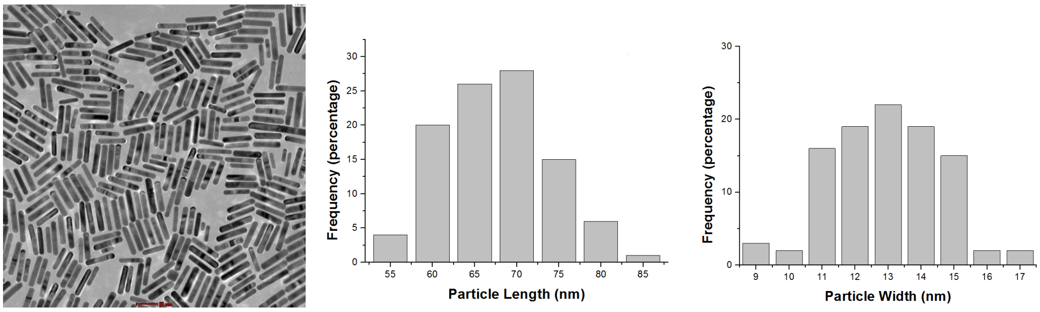

Figure S25. TEM micrographs and particle size distribution chart of GNP6. 50 particles were counted. $<d_{length}>$=67.5 nm, $<d_{width}>$=13 nm. Scale bar is 100 nm.

Table S17. Nanoparticle number concentration measured by Nanoparticle Tracking Analysis (NTA).

Sample Name	**Number Concentration (NP/mL)**
GNP1	1.26±0.027 E12
GNP2	1.17±0.272 E12
GNP3	9.60±0.747 E11
GNP4	8.67±0.679 E11
GNP5	6.33±0.212 E12
GNP6	3.43±0.421 E12

S4. Identification and Geometrical Characterisation of Nanoparticles From TEM Micrographs

What follows is the description of the computer software aimed to identify and process the anisotropic nanoparticles using 2D micrographs from TEM in a semi-automatic fashion. The idea was to use "ingredients" from different theories (percolation, cluster analysis, heuristic algorithms) in order to identify the nanoparticles automatically, allowing the user to revise and correct software identification easily.

Techniques used to build the software. The main steps to identify the nanoparticles are: *i)* identification of nanoparticle clusters and *ii)* separation of the nanoparticle clusters. To identify the clusters of nanoparticles we transformed the 2D image from TEM applying a threshold, obtaining a 2D matrix where each element may be either occupied or unoccupied, we then used the Hoshen-Kopelman algorithm[5] to identify clusters of contiguous cells. In Figure S26 a TEM image of the GNP4 is shown with a possible result of this step; the red contours are the identified clusters and some clusters have more than one branched gold nanoparticle.

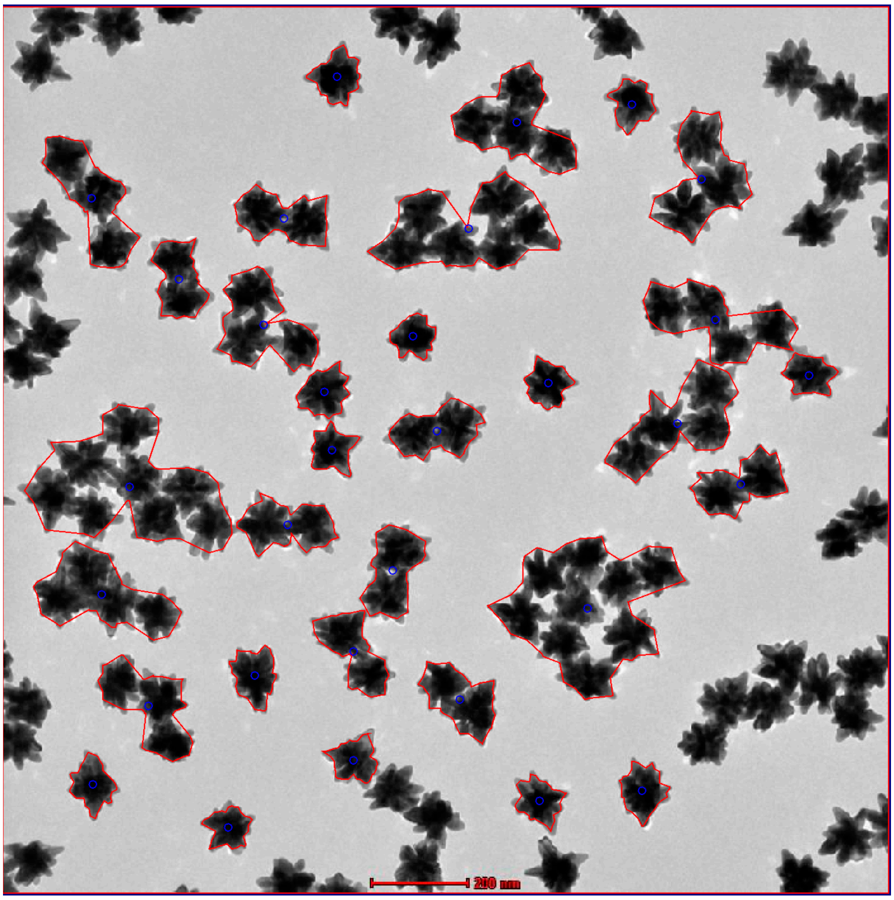

Figure S26. TEM image of GNP4 branched nanoparticles showing a first step in nanoparticle identification. After applying the threshold and Hoshen-Kolpeman algortihm the clusters of contiguous cells (red contours) are obtained.

The next step is the separation of the clusters. We tried several techniques, *i.e.* Watershed Transform[6] and k-means clustering algorithm[7, 8] obtaining the best results with the k-means clustering algorithm (Figure S27).

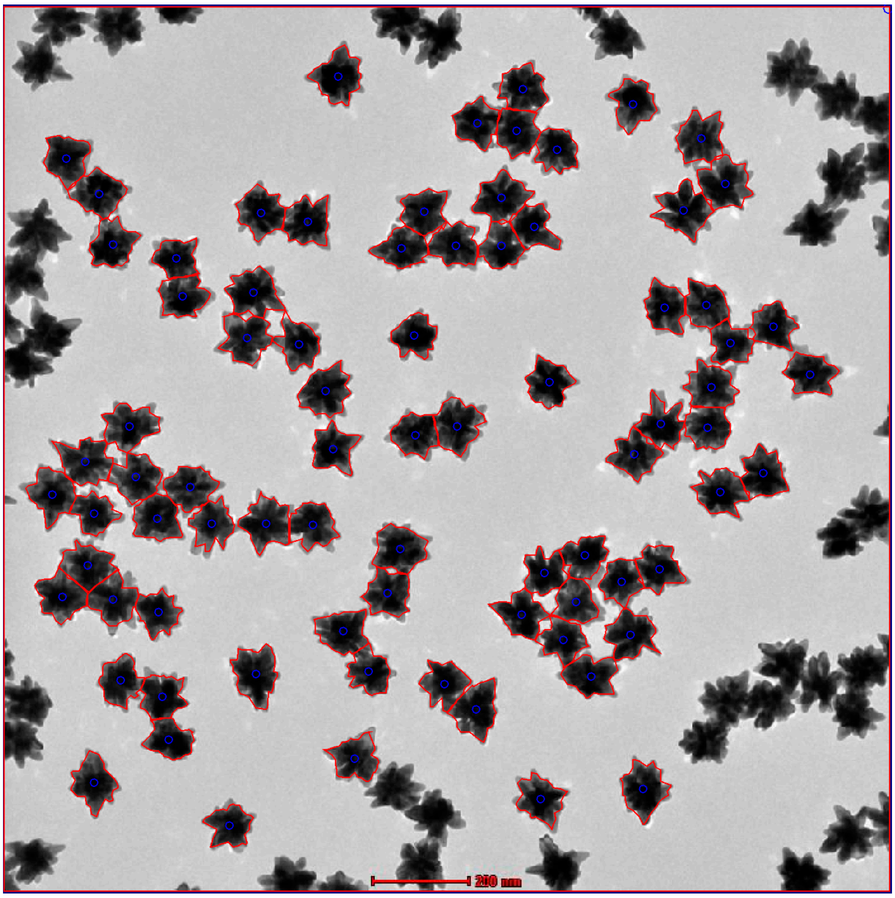

Figure S27. The same TEM image as in Figure S26 after cluster separation by k-means algorithm.

After identification and separation, we can use the identified nanoparticles to calculate the geometrical properties of interest like average size, area, perimeter, etc. The software is still under development but we were able to use it to characterize the branched gold nanoparticles in the present work.

References

1. Potenza, M. A. C.; Sanvito, T; Pullia, A. Measuring the complex field scattered by single submicron particles, *AIP Advances* **2015**, *5*, 117222.
2. Bohren, C. F., Huffman, D. R. Absorption and Scattering of Light by Small Particles. Wiley-VCH: Berlin, **1998**.
3. Hulst, H. C. v. d. Light Scattering by Small Particles. Dover, N.Y., **1981**.
4. Ashkroft, N. W.; Mermin, N. D. Solid State Physics, Harcourt College Publisher, **1976**.
5. Hoshen, J.; Kopelman, R. Percolation and cluster distribution. I. Cluster multiple labeling technique and critical concentration algorithm. *Phys. Rev. B* **1976**, *14*, 3438.
6. Russ, J. C. The image processing handbook (3rd ed.). CRC Press, Inc.: **1999**; p 771.
7. Hartigan, J. A. Clustering Algorithms. John Wiley; Sons, Inc.: **1975**; p 351.
8. MacQueen, J. In *Some methods for classification and analysis of multivariate observations*, Proceedings of the Fifth Berkeley Symposium on Mathematical Statistics and Probability, Volume 1: Statistics, Berkeley, Calif., 1967; University of California Press: Berkeley, Calif., **1967**; pp 281-297.